



## Experimental characterisation of neural tissue at collision speeds

Title	Experimental characterisation of neural tissue at collision speeds
Author(s)	Destrade, Michel;Rashid, Badar;Gilchrist, Michael
Publication Date	2012
Publisher	International Research Council on Biomechanics of Injury (IRCOBI)

## Experimental Characterisation of Neural Tissue at Collision Speeds

Badar Rashid<sup>1</sup>, Michel Destrade<sup>2</sup>, Michael D. Gilchrist<sup>3\*</sup>

\* Corresponding Author

**Abstract** Mechanical characterization of brain tissue at high loading velocities is particularly important for modelling Traumatic Brain Injury (TBI). During severe impact conditions, brain tissue experiences a mixture of compression, tension and shear. Diffuse axonal injury (DAI) occurs in animals and humans when both the strains and strain rates exceed 10% and 10/s, respectively. Knowing the mechanical properties of brain tissue at these strains and strain rates is of particular importance, as they can be used in finite element simulations to predict the occurrence of brain injuries under different impact conditions. In this research, we describe the design and operation of a High Rate Tension Device (HRTD) that has been used for tensile tests on freshly harvested specimens of porcine neural tissue at speeds corresponding to a maximum strain rate of 90/s. We investigate the effects of inhomogeneous deformation of the tissue during tension by quasi-static tests (strain rate 0.01/s) and dynamic tests (strain rate 90/s) using different thickness specimens (4.0, 7.0, 10.0 and 13.0 mm) of the same diameter (15.0 mm). Based on a combined experimental and computational analysis, brain specimens of aspect ratio (diameter/thickness)  $S = 10/10$  or lower ( $10/12$ ,  $10/13$ ) are considered suitable for minimizing the effects of inhomogeneous deformation during tension tests. The Ogden material parameters were derived from the experimental data both at quasi-static conditions ( $\mu = 440$  Pa and  $\alpha = -4.8$  at 0.01/s strain rate) and dynamic conditions ( $\mu = 4238$  Pa and  $\alpha = 2.8$  at 90/s strain rate) by performing an inverse finite element analysis to model all experimental data. These material parameters will prove useful for the nonlinear hyperelastic analysis of brain tissue.

**Keywords** Brain Tissue, Dynamic, Inhomogeneous, Traumatic Brain Injury (TBI)

### I. INTRODUCTION

During a severe impact to the head, brain tissue experiences a mixture of compression, tension and shear. *Diffuse axonal injury* (DAI) is the most severe form of injury, occurring at shear strains of approximately 10% – 50% and strain rates of approximately 10 – 50/s [1-8]. Access to the mechanical properties of brain tissue at these strains and strain rates is of particular importance, as they can be used in finite element simulations to predict the occurrence of brain injuries under variable impact conditions. In order to investigate the mechanisms involved in Traumatic Brain Injury (TBI), several research groups have investigated the brain's mechanical properties over a wide range of loading conditions by adopting different test protocols [1-6, 9-36]. However, to date, few tests have been performed in tension [37-39].

The Kolsky test apparatus is commonly used to perform compression tests at high strain rates, but it is more suitable for strain rates  $> 100/s$ . Based on the specific range of strain and strain rates which are injurious to axons during DAI, there is now an urgent need to develop a tensile test apparatus that can perform tests at strain rates up to 100/s. Cylindrical specimens are often used for testing brain tissue because of its fragile and tacky nature, and they are usually glued at the boundaries (brain/platen interface) as an alternative to clamping. This arrangement produces inhomogeneous deformation field near the boundaries (see Miller and Chinzei [37]). The end effects contribute to higher magnitudes of stresses, thus resulting in steeper stress – strain curves. They also preclude the use of analytical tension – stretch relations.

In this research, we describe the development and operation of a custom-designed High Rate Tension Device (HRTD) which is capable of performing tests at strain rates  $\leq 90/s$ . In the second phase of this research,

B. Rashid<sup>1</sup> is a PhD student in Mechanical & Materials Engineering at University College Dublin, Ireland. M. Destrade<sup>2</sup> is Prof. of Applied Mathematics in the School of Mathematics, Statistics and Applied Mathematics at NUI-Galway, Ireland. M.D. Gilchrist<sup>3</sup> is Head of the School of Mechanical & Materials Engineering at University College Dublin, Ireland. (phone: + 353 1 716 1890, fax: +353 1 283 0534, email: michael.gilchrist@ucd.ie).

an appropriate aspect ratio,  $S = (\text{diameter}/\text{thickness})$  of the specimen was determined in order to avoid any significant end effects due to inhomogeneous deformation of porcine brain tissue during tensile tests. Several tensile tests with variable sample thicknesses of 4.0, 7.0 and 10.0 mm were performed while maintaining a constant nominal diameter of 15.0 mm at strain rates of 0.01 and 90/s. The experimental data is also analyzed numerically as a nonlinear hyperelastic material by using the one-term Ogden material parameters  $(\mu, \alpha)$  in the ABAQUS Finite Element code. This research will provide further insight into the behavior of brain tissue and the feasibility of performing reliable tension experiments on suitably sized specimens of brain tissue.

## II. METHODS

### Experimental Setup

A High Rate Tension Device (HRTD) was developed to perform tests at variable loading velocities in order to investigate inhomogeneous deformation effects on brain tissue at different specimen thicknesses, as shown in Fig. 1. The major components of the apparatus include an *electronic actuator* (700 mm stroke, 1500 mm/s velocity, LEFB32T-700, SMC Pneumatics), two  $\pm 5$  N *load cells* (rated output: 1.46 mV/V nominal, GSO series, Transducer Techniques) and a *Linear Variable Displacement Transducer* (range  $\pm 25$  mm, ACT1000 LVDT, RDP Electronics). The load cells were calibrated against known masses and a multiplication factor of 13.67 N/V (determined through calibration) was used to convert voltage (V) to force (N). An integrated amplifier (AD 623 Gain,  $G = 100$ , Analog Devices) with built-in single pole low-pass filters having cut-off frequencies of 10 kHz and 16 kHz were used. The amplified signal was analyzed through a data acquisition system (DAS) with a sampling frequency of 10 kHz. The force (N) and displacement (mm) data against time (s) were recorded for the tissue experiencing 30% strain.

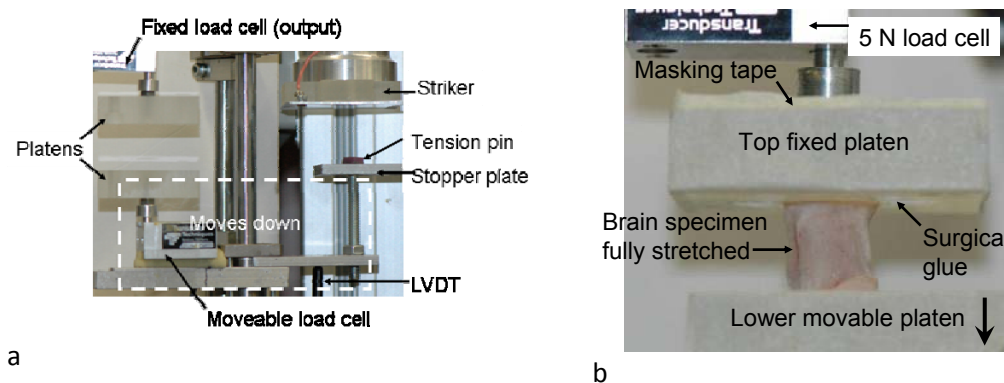


Fig. 1 (a). Major components of high rate tension device (HRTD) (b). fully stretched specimen after the test

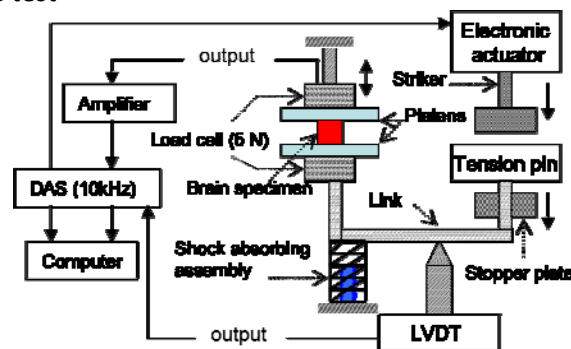


Fig. 2. Schematic diagram of complete test setup.

Reliably attaching brain tissue specimens to load cell platens was crucial in order to achieve high repeatability before operating HRTD at a particular velocity (see Fig 1 (b)). The surfaces of the platens were first covered with a masking tape substrate to which a thin layer of surgical glue (Cyanoacrylate, Low-viscosity Z105880-1EA, Sigma-Aldrich) was applied. The prepared cylindrical specimen of tissue was then placed on the lower platen. The top platen, which was attached to the 5 N load cell, was then lowered slowly so as to just touch the top surface of the specimen. One minute settling time was sufficient to ensure proper adhesion of the specimen to

the platens. High speed image recording of brain tissue during tension tests was done at a frame rate of 3906 fps with 640 x 480 resolutions by using a high speed digital camera (Phantom V5.1, CMOS 10 bit Sensor, 1200 frames per second (fps)). The images were examined to inspect that the cylindrical brain samples were uniformly deformed and the faces of the specimen were firmly bonded to the moving and stationary platens during extension of the brain specimen.

The *striker* attached to the electronic actuator moved at a particular velocity to strike the *tension pin* which was rigidly attached to the lower platen through a rigid *link* as shown in Fig. 2. During the tests, the top platen remained stationary while the lower platen moved down to produce the required tension in the specimen. The two output signals (displacement signal from LVDT and force signal from the load cell), as shown in Fig. 2, were captured simultaneously through the data acquisition system (DAS) at a sampling rate of 10 kHz. The pre-stressed *LVDT probe* was in continuous contact with the *link* to sense the displacement signal during the tension phase of tests. Two main contributing factors for the non-uniform velocity were the deceleration of the electronic actuator when it approached the end of the stroke and the opposing forces acting against the striking mechanism. Therefore, the striking mechanism was designed and adjusted to ensure that it impacted the tension pin approximately 150 mm before the actuator came to a complete stop. The *striker* impact generated backward thrust, which was fully absorbed by the spring mounted on the actuator guide rod to prevent any damage to the *programmable servo motor*.

### Calibration and Loading Velocities

Calibration of the HRTD was essential in order to ensure uniform velocity during extension of brain tissue at each strain rate. During the calibration process, the actuator was run several times with and without any brain tissue specimen to ensure repeatability of displacement (mm) against time (s). Once it was established that the actuator was capable of providing the required uniform velocity, brain tissue specimen was then mounted on the HRTD for the actual tests. In order to maintain a constant strain rate with variable specimen thickness, the machine velocity was varied at each thickness. The required velocities for each specimen thickness and the achieved velocities at strain rates of 0.01 and 90/s are shown in Table 1. A standard Tinius Olsen material testing machine (maximum speed: 500 mm/min) was used for tests at a strain rate of 0.01/s.

TABLE 1  
LOADING VELOCITIES UP TO 30% STRAIN

Strain rate (1/s)	Specimen thickness (mm)	Required velocity (mm/s)	Achieved velocity (mm/s) $\pm$ SD
0.01	4	0.04	0.04 $\pm$ 0.008
	7	0.07	0.07 $\pm$ 0.004
	10	0.10	0.10 $\pm$ 0.007
	13	0.13	0.13 $\pm$ 0.005
90	4	360	359 $\pm$ 1.3
	7	630	630 $\pm$ 1.1
	10	900	899 $\pm$ 1.2

### Specimen Preparation Procedure

Ten fresh porcine brains from approximately six month old pigs were collected from a local slaughter house and tested within 3 h postmortem. Each brain was preserved in a physiological saline solution at 4 to 5°C during transportation. As shown in Fig. 3, one half of the cerebral hemisphere was cut in the coronal plane to extract two coronal slices. Cylindrical specimens composed of mixed white and gray matter of nominal thicknesses of 4.0, 7.0, 10.0 and 13.0 mm and 15.0 mm diameter were prepared. A circular steel die cutter of 15.3 mm diameter was used to prepare nearly perfect circular specimens that were then inserted in cylindrical metal disks with thickness of 4.1, 7.1, 10.1 and 13.1 mm but with the same internal diameter of 15.2 mm. Any excessive brain portion was then removed with a surgical scalpel. The scalpel was dipped in a saline solution

before cutting brain tissue to avoid sticking. The actual brain specimen diameter was  $15.1 \pm 0.1$  mm and the thickness was  $4.0 \pm 0.1$  mm,  $7.0 \pm 0.1$  mm,  $10.0 \pm 0.1$  mm, and  $13.0 \pm 0.1$  mm (mean  $\pm$  SD). A visible contraction of the samples occurred immediately after they were removed from the brains, revealing the presence of residual stresses *in-vivo*. When measuring the dimensions of the specimens, it was noted that the nominal dimensions were reached after a few minutes; it was at this stage that the testing commenced. 80 specimens were excised from 10 porcine brains (8 specimens from each brain) and tested at a nominal room temperature of 22 °C. The time elapsed between harvesting of the first and the last specimens from each brain was 13 ~ 16 minutes. Due to the extreme softness and tackiness of brain tissue, each specimen was tested only once and no preconditioning was done [21, 23, 37, 39].

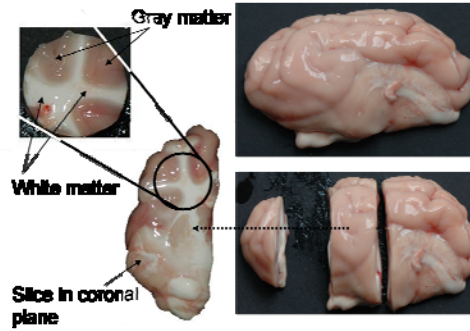


Fig. 3. Extraction of cylindrical specimens from the porcine brain tissue containing mixed white and gray matter

### Hyperelastic Constitutive Modelling

In general, an isotropic hyperelastic incompressible material is characterized by a strain-energy density function  $W$  which is a function of two principal strain invariants only:  $W = W(I_1, I_2)$ , where  $I_1$  and  $I_2$  are defined as [40],

$$I_1 = \lambda_1^2 + \lambda_2^2 + \lambda_3^2, \tag{1}$$

$$I_2 = \lambda_1^2 \lambda_2^2 + \lambda_1^2 \lambda_3^2 + \lambda_2^2 \lambda_3^2. \tag{2}$$

Here  $\lambda_1^2, \lambda_2^2, \lambda_3^2$  are the squares of the principal stretch ratios, linked by the relationship  $\lambda_1 \lambda_2 \lambda_3 = 1$ , due to incompressibility. During the experimental tension tests, the principal stretch ratio  $\lambda$  was calculated from the measure of the elongation  $e$ , i.e.,  $\lambda = 1 + e$ . The nominal stress component along the direction of tension  $S$  was evaluated as  $S \equiv F / A$ , where  $F$  is the tension force, as measured in Newtons by the load cell, and  $A$  is the area of a cross section of the sample in its undeformed state. The experimentally measured nominal stress was then compared to the predictions of the hyperelastic models from the following relation [40], valid for homogeneous tensile tests

$$S_{33} = \frac{d\tilde{W}}{d\lambda}, \text{ where } \tilde{W}(\lambda) \equiv W(\lambda^2 + 2\lambda^{-1}, \lambda^{-2} + 2\lambda), \tag{3}$$

Due to symmetry and incompressibility, the stretch ratios are of the form

$$\lambda_1 = \lambda, \quad \lambda_2 = \lambda_3 = \frac{1}{\sqrt{\lambda}},$$

### Ogden Strain Energy Function

The Ogden model [41] has been used in the past to describe the nonlinear mechanical behavior of the brain, as well as of other nonlinear soft tissues [16, 37, 39, 42, 43]. Soft biological tissue is often modeled well by the Ogden formulation and most of the mechanical test data available for brain tissue in the literature are fitted with an Ogden hyperelastic function. The one-term Ogden hyperelastic function is given by [16]

$$W = \frac{2\mu}{\alpha^2} (\lambda_1^\alpha + \lambda_2^\alpha + \lambda_3^\alpha - 3), \tag{4}$$

where  $\mu > 0$  is the infinitesimal shear modulus (Pa), and  $\alpha$  is a large-strain stiffening parameter. It yields the following nominal stress  $S_{33}$ , in the case of a homogeneous tensile test,

$$S_{33} = \frac{2\mu}{\alpha} \left\{ \lambda^{\alpha-1} - \lambda^{-\left(\frac{\alpha}{2}+1\right)} \right\} \tag{5}$$

It was not possible to achieve perfect homogeneous deformation conditions during tension tests due to the bonding of brain tissue (no slip conditions) at the platen/brain interfaces [44]. This was considered to be a practical limitation of our experimental protocol. Nevertheless, an effort was made to select an appropriate specimen aspect ratio,  $S$  (diameter/thickness) which would produce negligible inhomogeneous deformation effects due to the no slip boundary conditions.

### III. RESULTS

#### Experimentation

Ten tensile tests were performed at each nominal specimen thickness (4.0, 7.0 and 10.0 mm) up to 30% strain both at quasi static (0.01/s) and dynamic (90/s) strain rates, however the diameter of each specimen was always 15.0 mm. Tests were also performed at a nominal specimen thickness of 13.0 mm in order to further analyze inhomogeneous deformation of brain tissue in tension at a low strain rate of 0.01/s. All tests were conducted at a nominal room temperature of 22°C. Standard Tinius Olsen material testing machine was used to perform tests at a low strain rate of 0.01/s and the Force (N) and displacement (mm) data was measured directly; this was converted to engineering stress (Pa) – strain for each specimen thickness as shown in Fig. 4. Similarly, dynamic tests were performed at 90/s strain rate using the HRTD and the data was measured directly through the data acquisition system (Handyscope, HS4) at a sampling frequency of 10 kHz; and the resulting data at each specimen thickness is shown in Fig. 5.

It is to be noted that the stresses are significantly higher for the thinner specimens than for the thicker specimens at the same strain rate. It is also observed statistically, using a one-way ANOVA test, that there is a significant difference between the stresses associated with the 4.0 and 7.0 mm specimen thicknesses ( $p = 0.00243$ ) and similarly ( $p = 0.09188$ ) between those of the 7.0 and 10.0 mm specimen thicknesses at 0.01/s strain rate. Similarly at 90/s strain rate, between 4.0 and 7.0 mm specimen thicknesses ( $p = 0.09610$ ) and between 7.0 and 10.0 mm specimen thicknesses ( $p = 0.18936$ ). The higher magnitudes of stresses are due to the restrictions imposed on the specimens at the boundaries (brain/platen interface) because of the attachment to the platens using surgical glue. Because of this restriction, the tissue deformation near the platen ends is inhomogeneous, thus resulting in steeper stress – strain curves, particularly for thinner specimens. It is also observed that the experimental engineering stress profile in the case of 90/s strain rate shows a significantly stiffer behavior (Fig. 7) as compared to a low strain rate of 0.01/s, which is convex upward as clearly depicted in Fig. 6. A similar behavior of porcine brain tissue at low loading velocities was also observed by Miller and Chinzei [37]. The engineering stresses at 30% strain at the nominal specimen thicknesses of 4.0, 7.0, 10.0 and 13.0 mm are  $454.2 \pm 122.5$  Pa,  $302 \pm 40.5$  Pa,  $232 \pm 38.5$  Pa,  $220 \pm 65.7$  Pa (mean  $\pm$  SD), respectively at the 0.01/s strain rate. The engineering stresses at 30% strain at the nominal specimen thicknesses of 4.0, 7.0 and 10.0 mm are  $5.36 \pm 0.69$  kPa,  $4.1 \pm 0.76$  kPa,  $3.3 \pm 0.52$  kPa (mean  $\pm$  SD), respectively at 90/s strain rate.

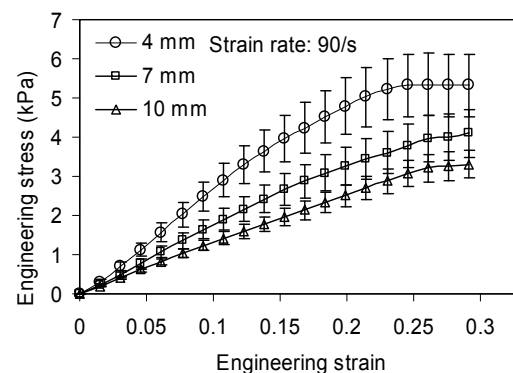
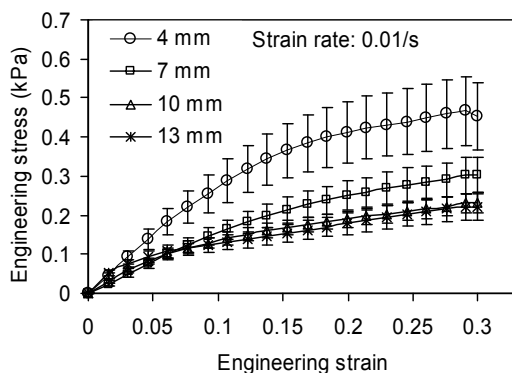


Fig.4. Experimental engineering stress (Pa) profiles with error bars showing standard deviation (at 0.01/s)

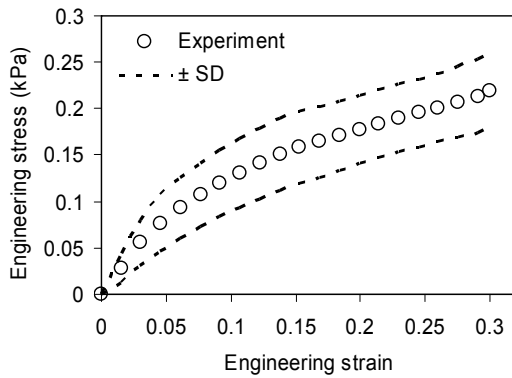


Fig.6. Experimental engineering stress (Pa) profile at 0.01/s strain rate

Fig.5. Experimental engineering stress (kPa) profiles with error bars showing standard deviation (at 90/s)

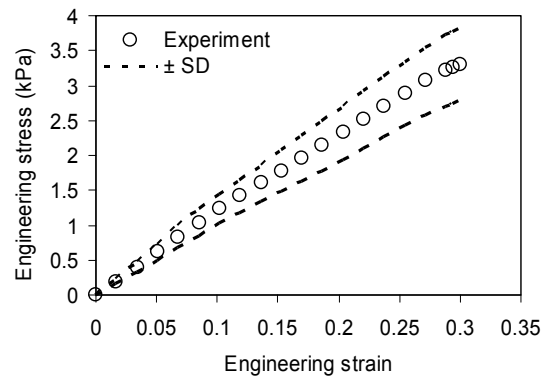


Fig.7. Experimental engineering stress (kPa) profile at 90/s strain rate

**Finite Element Simulations**

At this stage, it was informative to carry out numerical analysis using ABAQUS 6.9/Explicit in order to investigate further the effects of variable specimen thickness (4.0, 7.0, 10.0, 11.0, 12.0, 13.0, 14.0 mm). Various boundary conditions were applied to mimic experimental conditions. One end of the cylindrical specimen was constrained in all directions whereas the other end was stretched up to 30% strain. Mass density was determined experimentally during this study and found to be  $1040 \pm 1 \text{ kg/m}^3$ , which is similar to, Velardi et al. [39] who used a mass density of 1039 and 1036  $\text{kg/m}^3$  for the white matter and the gray matter, respectively. C3D8R elements (hexagonal, 8-node linear brick with reduced integration) were used in the simulations. Experimental data at a low strain rate of 0.01/s was used to derive Ogden material parameters ( $\mu = 440 \text{ Pa}$ ,  $\alpha = -4.8$ ) by performing an inverse finite element analysis. The derived material parameters converged to average experimental engineering stress (Pa) – stretch data obtained at different specimen thicknesses (4.0, 7.0, 10.0 and 13.0 mm). This procedure was particularly important to ensure that the resulting material parameters were the same irrespective of specimen thickness. The same procedure was adopted to estimate material parameters ( $\mu = 4238.0 \text{ Pa}$ ,  $\alpha = 2.8$ ) from the experimental data at a strain rate of 90/s. The derived nonlinear hyperelastic parameters were kept the same for all the simulations performed at various specimen thicknesses.

**Solution Convergence Approach**

After determining experimental engineering stress (Pa) – stretch data, curve fitting was performed using data obtained from the maximum specimen thickness (13.0 mm). This procedure provides initial starting values of  $\mu$  and  $\alpha$  as material parameters for the simulation in ABAQUS/ 6.9, software. The results from the FE simulations were then compared with experimental results pertaining to each specimen thickness (4.0, 7.0, 10, 13.0 mm). The convergence of FE data to experimental data was assessed based on Coefficient of determination

$$R^2 = 1 - \frac{S_r}{S_t}$$

where  $S_r$  = total sum of squared distances between the experimental and FE stress profiles and

$S_t$  = total sum of squared distances between the experimental stresses and their mean. The values of  $\mu$  and  $\alpha$  were updated in each iteration and simulations continued until  $R^2$  was approximately equal to 0.9980 in order to achieve good agreement between the experimental and numerical stresses. The material parameters were input manually into the ABAQUS 6.9 for each simulation.

A mesh convergence analysis was carried out by varying mesh density. In our study, we regarded the mesh as being convergent when there was a negligible change in the numerical solution (0.8%) with further mesh refinement. We achieved convergence with 2016 to 3172 elements for the 4 to 13.0 mm thick specimens of diameter 15.0 mm, respectively. The average simulation time for these models was 60s. We also analyzed the *accumulated artificial strain energy* used to control *hourglass deformation* during numerical simulations. It was observed that the *artificial strain energy* for the whole model, as a percentage of the *total strain energy*, was

within the range of 1.46 – 3.1%. The significance of this low proportion of artificial strain energy ( $\leq 3.1\%$ ) indicates that *hourglassing* is not a problem.

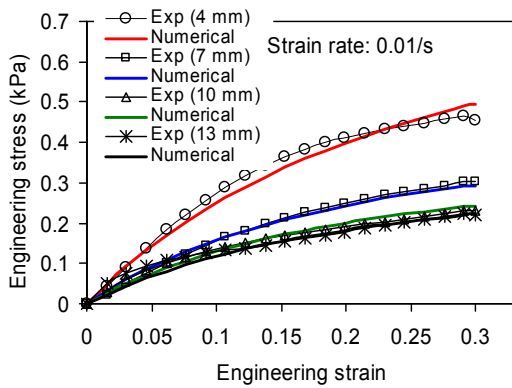


Fig.8. Excellent agreement of numerical stress with average experimental stress (at 0.01/s)

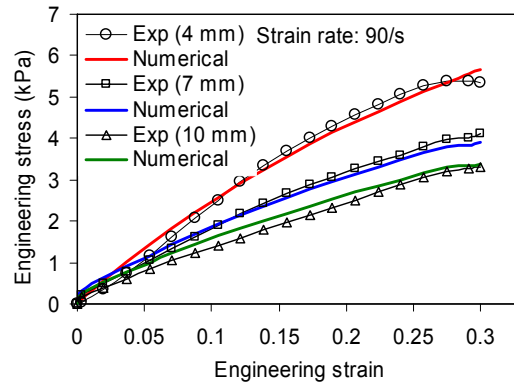


Fig.9. Excellent agreement of numerical stress with average experimental stress (at 90/s)

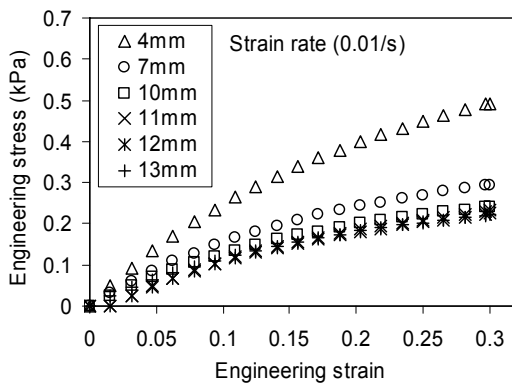


Fig.10. Numerical engineering stresses at variable specimen thickness; 0.01/s strain rate

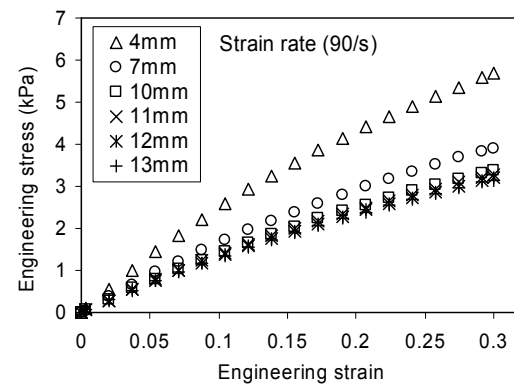


Fig.11. Numerical engineering stresses at variable specimen thickness; 90/s strain rate

Excellent agreement between the numerical engineering stress and the average experimental engineering stress profiles is achieved, as shown in Fig. 8 and 9. Based on one way ANOVA test,  $p = 0.8962$  at 4.0 mm,  $p = 0.9544$  at 7.0 mm,  $p = 0.9242$  at 10.0 mm and  $p = 0.8366$  at 13.0 mm at quasi static loading conditions. Similarly,  $p = 0.9595$  at 4.0 mm,  $p = 0.9252$  at 7.0 mm and  $p = 0.7581$  at 10.0 mm at dynamic conditions. It is observed numerically and experimentally that the magnitudes of stresses are significantly higher with the reduction in specimen thickness or at higher aspect ratio,  $S$  (diameter/thickness). The analysis was further extended to higher specimen thicknesses (11.0 to 13.0 mm) particularly at a strain rate of 90/s. The stresses are significantly reduced with the increase in specimen thickness at both the strain rates of 0.01/s and 90/s as shown in Fig. 10 and 11. Based on a one-way ANOVA statistical analysis, it is found that there is no significant difference ( $p = 0.8467$ ) in the stress magnitudes between the thickest specimens (10.0 – 13.0 mm at 0.01/s strain rate) i.e., at low aspect ratios ( $S = 1.5 - 1.15$ ). Similarly, there is no significant difference between the stresses associated with the thick specimens (10.0 – 13.0 mm) at 90/s strain rate ( $p = 0.9845$ ).

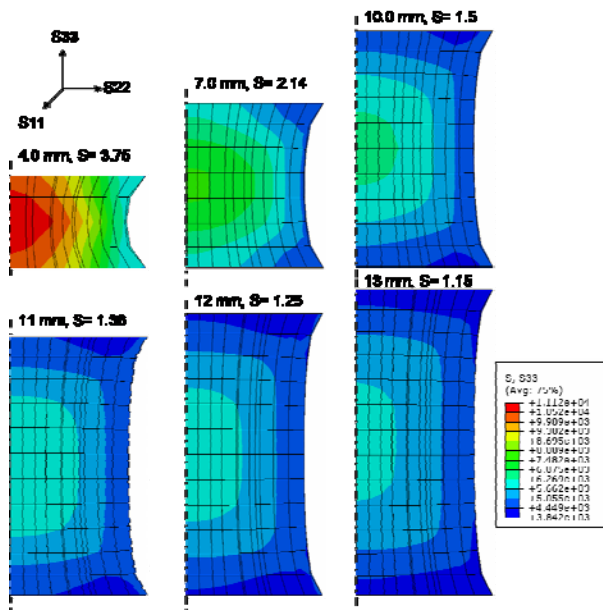


Fig. 12. Distribution of stresses (Pa) at variable specimen thickness or aspect ratio,  $S = \text{diameter/height}$  (3.75 – 1.15) using 15.0 mm diameter at 90/s strain rate

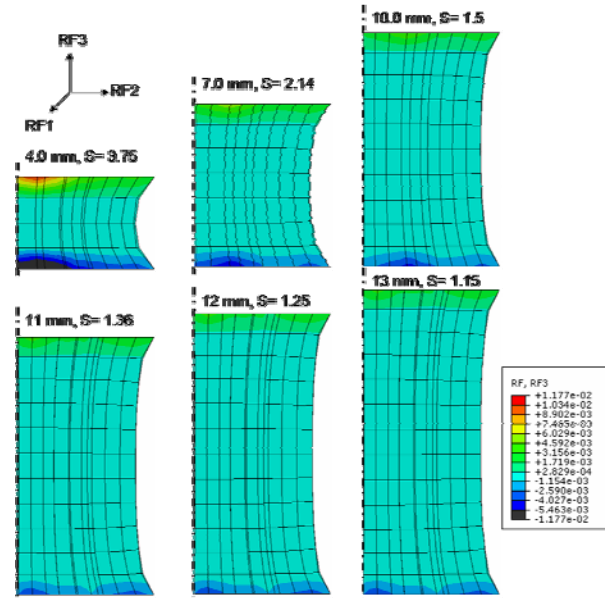


Fig. 13. Distribution of forces (N) at variable specimen thickness or aspect ratio,  $S = \text{diameter/height}$  (3.75 – 1.15) using 15.0 mm diameter at 90/s strain

The distribution of numerical stresses (Pa) and forces (N) were analyzed using Ogden hyperelastic parameters at a dynamic strain rate of 90/s ( $\mu = 4238.0 \text{ Pa}$ ,  $\alpha = 2.8$ ) while doing simulations in ABAQUS 6.9/Explicit at variable specimen thicknesses as shown in Figs 12 and 13. However, similar distributions of numerical stresses and forces was also observed at quasi static conditions. It is clearly observed that a more homogeneous stress and force pattern is achieved at an aspect ratio of  $S$  (diameter/thickness)  $\leq 1.5$ . However, the numerical stresses and forces are significantly higher in the case of the 4.0 mm thick specimen, as depicted in Figs 12 and 13. It is to be noted that inhomogeneous forces exist at the ends of the specimen (platen ends or brain/platen interface) as depicted in Fig. 13. The effects of these forces are significantly reduced at an aspect ratio,  $S \leq 1.5$ .

**Aspect Ratio Analysis**

So far we have carried out experimental and numerical analysis by varying specimen thickness only, while maintaining the same diameter (15.0 mm). However, the diameter of the test sample is also an important factor to be considered when determining the effects of inhomogeneous deformation. Therefore, numerical simulations were performed at 15.0 and 20.0 mm diameters for each specimen thickness (4.0, 7.0, 10.0 and 13.0 mm). The material parameters ( $\mu = 4238.0 \text{ Pa}$ ,  $\alpha = 2.8$ ) from the tests conducted at dynamic strain rates (90/s) were used for this analysis. However, similar behavior was expected for the quasi static conditions. Stiffening behavior is observed with larger specimen diameters; however this effect is significantly reduced at the larger specimen thickness of 13.0 mm, as shown in Fig. 14. The larger diameter produces more inhomogeneous deformation which contributes to the higher stress magnitudes. The difference between the stress profiles at aspect ratios,  $S = 10/10$  and  $10/13$  was also analyzed statistically using a one-way ANOVA test ( $p = 0.8094$ ). The stress magnitudes are slightly higher (7.3%) in case of  $S = 15/10$  as compared to  $S = 10/10$ .

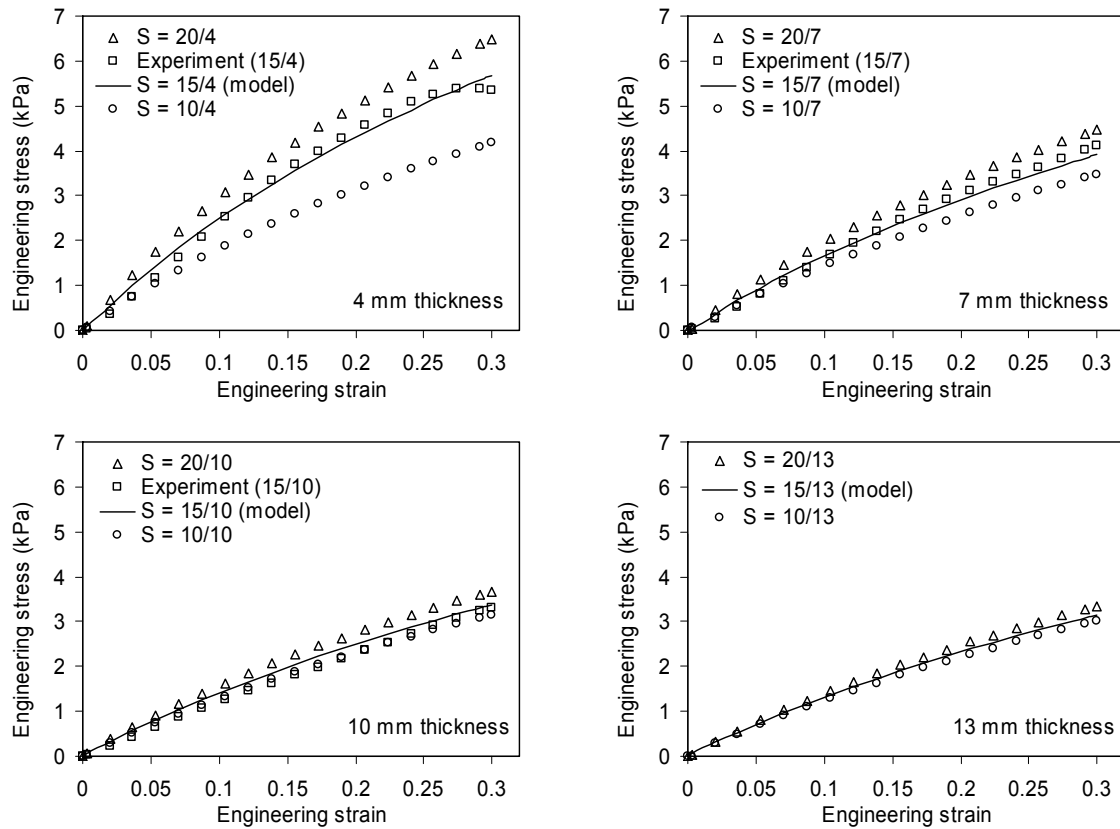


Fig. 14. Variation in engineering stress profiles at different aspect ratios,  $S = \text{diameter/thickness}$ . The effects of larger specimen diameter are significantly reduced at 13.0 mm thick specimen

#### IV. DISCUSSION

In this research an effort has been made to determine a suitable thickness for cylindrical brain specimens in order to derive reliable experimental data during tensile tests. This aspect of our experimental protocol was vital to investigate because of the inhomogeneous deformation of brain tissue near the boundaries (brain/platen interface) as a result of the fixed attachment to the platens using surgical glue. The end effects contribute to higher magnitudes of stresses, thus resulting in steeper stress – strain curves [44]. It was observed that the tensile stresses of the brain tissue are significantly different at variable specimen thicknesses ( $\leq 10.0$  mm). Moreover, during the analysis, it was revealed that the larger aspect ratio specimens do not have a sufficiently uniform stress distribution to provide meaningful results. The experimental results were further validated by finite element analysis using Ogden hyperelastic material parameters.

It is noted that Miller and Chinzei [37] used cylindrical samples of diameter 30.0 mm and height 10.0 mm ( $S = 3$ ) during tensile tests at quasi-static velocities (0.005, 5.0 and 500 mm/min), whereas in compression tests they used a sample height of 13 mm ( $S = 2.3$ ). Tamura et al [38] on the other hand, performed tensile tests at 0.9, 4.3 and 25/s strain rates using cylindrical specimens of diameter  $\sim 14.0$  mm and height  $\sim 14.0$  mm ( $S = 1.0$ ). The magnitudes of the engineering stress reported by Miller and Chinzei at a strain rate of 0.0064/s, using 10.0 mm thick specimen during tensile tests is of the same order of magnitude as estimated in the present study at a strain rate of 0.01/s. The engineering stress profile was observed to be convex upward during quasi static loading conditions (0.01/s) at a specimen thickness of 10.0 mm and above; similar behavior was observed by Miller and Chinzei [37]. A one-term Ogden strain energy function was sufficient to model data at strain rates of 0.01/s and 90/s, as depicted in Fig. 8 and 9.

To the best of the authors’ knowledge, there is no experimental data available in tension at 90/s strain rate for comparison purpose. However, special attention was paid to calibrating the *High Rate Tension Device (HRTD)* in order to obtain precise data. The achieved velocities mentioned in Table 1 indicate that the HRTD was fully capable of attaining the required strain rates. Moreover, surgical glue provided reliable attachment of brain specimens to the platens. All tests were completed within 3 h of postmortem at a nominal room temperature of 22° C in order to maintain the inherent stiffness of the brain tissue. Our experimental protocol is fundamentally

similar to Miller and Chinzei [37], except for the addition of HRTD for the dynamic tests, therefore experimental data presented in this study can be considered reliable. The results of finite element simulations performed by using one-term Ogden model were also in good agreement with the experimental data, as clearly depicted in Figures 8 and 9.

Based on the present analysis, it was determined that cylindrical specimens of aspect ratio  $S = 10/10$  or lower ( $10/11$ ,  $10/12$ ,  $10/13$ ) are suitable to perform tensile tests on brain tissue. The effects of specimen diameter are significantly reduced at 10.0 mm thick specimens and above. The brain tissue is rate dependent [16, 21-23, 36-38, 45-46] as observed during the experimentation at strain rates of 0.01/s and 90/s; this requires a hyperviscoelastic model to fully characterize the behavior of tissue. However, in this research we were mainly interested in investigating the inhomogeneous deformation of brain tissue during tension tests by varying specimen thickness; which was possible by adopting either a linear elastic, hyperelastic or viscoelastic approach.

## V. CONCLUSIONS

There are three important conclusions from this work.

- (i) We have presented the development and calibration of a custom designed HRTD that is useful to obtain experimental data at strain rates of up to 90/s.
- (ii) We found that a brain specimen aspect ratio  $S = 10/10$  or lower ( $10/11$ ,  $10/12$ ,  $10/13$ ) is suitable for the tensile tests.
- (iii) We have observed that a one-term Ogden strain energy function is appropriate to model the mechanical response of brain tissue under quasi static and dynamic conditions and the material parameters (at a strain rate of 0.01/s,  $\mu = 440$  Pa and  $\alpha = -4.8$ ; at a strain rate of 90/s,  $\mu = 4238.0$  Pa and  $\alpha = 2.8$ ) can be used for the nonlinear hyperelastic modeling of brain tissue.

## VI. ACKNOWLEDGEMENTS

We are grateful to Professor Alojz Ivankovic (UCD) for his valuable discussions. This work was supported for the first author by a Postgraduate Research Scholarship awarded in 2009 by the Irish Research Council for Science, Engineering and Technology (IRCSET), Ireland.

## VII. REFERENCES

- [1] Bain AC, Meaney DF. Tissue-level thresholds for axonal damage in an experimental model of central nervous system white matter injury. *J Biomech Eng.* 2000;122:615 – 22.
- [2] Bayly PV, Black EE, Pedersen RC. *In vivo* imaging of rapid deformation and strain in an animal model of traumatic brain injury. *J Biomech.* 2006;39:1086 – 95.
- [3] Morrison III B, Meaney DF, Margulies SS, McIntosh TK. Dynamic mechanical stretch of organotypic brain slice cultures induces differential genomic expression: relationship to mechanical parameters. *J Biomech Eng.* 2000;122:224 – 30.
- [4] Morrison III B, Cater HL, Wang CC, Thomas FC, Hung CT, Ateshian GA, et al. A tissue level tolerance criterion for living brain developed with an *In Vitro* model of traumatic mechanical loading. *Stapp Car Crash J* 2003;47:93-105.
- [5] Morrison III B, Cater HL, Benham CD, Sundstrom LE. An *in vitro* model of traumatic brain injury utilizing two-dimensional stretch of organotypic hippocampal slice cultures. *J Neurosci Methods.* 2006;150:192–201.
- [6] Pfister BJ, Weihs TP, Betenbaugh M, Bao G. An *in vitro* uniaxial stretch model for axonal injury. *Ann Biomed Eng* 2003;31:589–98.
- [7] Geddes MD, Cargill II RS. An *in vitro* model of neural trauma: Device characterization and calcium response to mechanical stretch. *J Biomech Eng.* 2001;123:247-55.
- [8] LaPlaca MC, Cullen DK, McLoughlin JJ, Cargill II RS. High rate shear strain of three-dimensional neural cell cultures: a new *in vitro* traumatic brain injury model. *J Biomech.* 2005;38:1093–105.

- [9] Arbogast KB, Thibault KL, Pinheiro BS, Winey KI, Margulies SS. A high-frequency shear device for testing soft biological tissues. *J Biomech.* 1997;30:757–9.
- [10] Bilston LE, Liu Z, Phan-Tiem N. Large strain behavior of brain tissue in shear: some experimental data and differential constitutive model. *Biorheology.* 2001;38:335–45.
- [11] Darvish KK, Crandall JR. Nonlinear viscoelastic effects in oscillatory shear deformation of brain tissue. *Med Eng Phy.* 2001;23:633–45.
- [12] Fallenstein GT, Hulce VD, Melvin JW. Dynamic mechanical properties of human brain tissue. *J Biomech.* 1969;2:217-26.
- [13] Hrapko M, van Dommelen JAW, Peters GWM, Wismans JSHM. The mechanical behaviour of brain tissue: large strain response and constitutive modelling. *Biorheology.* 2006;43(5):623–36.
- [14] Nicolle S, Lounis M, Willinger R. Shear properties of brain tissue over a frequency range relevant for automotive impact situations: New experimental results. *Stapp Car Crash J.* 2004;48:239 – 58.
- [15] Nicolle S, Lounis M, Willinger R, Palierne JF. Shear linear behavior of brain tissue over a large frequency range. *Biorheology.* 2005;42(3):209–23.
- [16] Prange MT, Margulies SS. Regional, directional, and age-dependent properties of the brain undergoing large deformation. *J Biomech Eng.* 2002;124(2):244–52.
- [17] Shuck LZ, Advani SH. Rheological response of human brain tissue in shear. *ASME, J Basic Eng.* 1972;94:905 - 11.
- [18] Thibault KL, Margulies SS. Age-dependent material properties of the porcine cerebrum: Effect on pediatric inertial head injury criteria. *J Biomech.* 1998;31:1119-26.
- [19] Cheng S, Bilston LE. Unconfined compression of white matter. *J Biomech.* 2007;40:117–24.
- [20] Estes MS, McElhaney JH. Response of brain tissue of compressive loading. *ASME.* 1970:Paper No. 70-BHF-13.
- [21] Miller K, Chinzei K. Constitutive modelling of brain tissue: experiment and theory. *J Biomech.* 1997;30(11-12):1115 -21.
- [22] Pervin F, Chen WW. Dynamic mechanical response of bovine grey matter and white matter brain tissues under compression. *J Biomech.* 2009;42:731–5.
- [23] Tamura A, Hayashi S, Watanabe I, Nagayama K, Matsumoto T. Mechanical characterization of brain tissue in high-rate compression. *J Biomech Sci Eng* 2007;2(3):115 - 26.
- [24] Arbogast KB, Margulies SS. Material characterization of the brainstem from oscillatory shear tests. *J Biomech.* 1998;31:801-7.
- [25] Brands DWA, Bovendeerd PHM, Peters GWM, Wismans JSH. The large shear strain dynamic behavior of In-vitro porcine brain tissue and the silicone gel model material. *Proceedings of the 44th Stapp Car Crash Conference* 2000:249–60.
- [26] Donnelly BR, Medige J. Shear properties of human brain tissue. *J Biomech Eng.* 1997;119(4):423–32.
- [27] Elkin BS, Ilankovan AI, Morrison III B. A detailed viscoelastic characterization of the P17 and adult rat brain. *J Neurotrauma.* 2011;28(11):2235-44.
- [28] Elkin BS, Ilankovan AI, Morrison III B. Dynamic, regional mechanical properties of the porcine brain:

Indentation in the coronal plane. *J Biomech Eng.* 2011;133:071009.

[29] Finan JD, Elkin BS, Pearson EM, Kalbian IL, Morrison III B. Viscoelastic properties of the rat brain in the sagittal plane: Effects of anatomical structure and age. *Ann Biomed Eng.* 2012;40(1):70-8.

[30] Galford JE, McElhaney JH. A viscoelastic study of scalp, brain and dura. *J Biomech.* 1970;3:211–21.

[31] Garo A, Hrapko M, van Dommelen JAW, Peters GWM. Towards a reliable characterization of the mechanical behaviour of brain tissue: The effects of postmortem time and sample preparation. *Biorheology.* 2007;44:51-8.

[32] Takhounts EG, Crandall JR, Darvish KK. On the importance of nonlinearity of brain tissue under large deformations. *Stapp Car Crash J.* 2003;47:107–34.

[33] van Dommelen JAW, van der Sande TJP, Hrapko M, Peters GWM. Mechanical properties of brain tissue by indentation: Interregional variation. *J Mech Behavior Biomed Mat.* 2010;3:158-66

[34] Bilston LE, Liu Z, Phan-Thien N. Linear viscoelastic properties of bovine brain tissue in shear. *Biorheology.* 1997;34(6):377-85.

[35] Arbogast K, Meaney D, Thibault L. Biomechanical characterization of the constitutive relationship for the brainstem. *SAE Technical Paper.* 1995 1995-11-01;952716.

[36] Rashid B, Destrade M, Gilchrist MD. Mechanical characterization of brain tissue in compression at dynamic strain rates. *J Mech Behavior Biomed Mat* 2012;10:23-38.

[37] Miller K, Chinzei K. Mechanical properties of brain tissue in tension. *J Biomech* 2002;35:483-90.

[38] Tamura A, Hayashi S, Nagayama K, Matsumoto T. Mechanical characterization of brain tissue in high-rate extension. *J Biomech Sci Eng* 2008;3(2):263 – 74.

[39] Velardi F, Fraternali F, Angelillo M. Anisotropic constitutive equations and experimental tensile behavior of brain tissue. *Biomech Model Mechanobiol* 2006;5(1):53–61.

[40] Ogden RW. *Non-linear elastic deformations.* New York: Dover 1997.

[41] Ogden RW. Large deformation isotropic elasticity—on the correlation of theory and experiment for incompressible rubber like solids. *Proc R Soc Lond A Math Phys Sci* 1972;326:565–84.

[42] Brittany C, Margulies SS. Material properties of porcine parietal cortex. *J Biomech.* 2006;39:2521–5.

[43] Lin DC, Shreiber DI, Dimitriadis EK, Horkay F. Spherical indentation of soft matter beyond the Hertzian regime: numerical and experimental validation of hyperelastic models. *Biomech Model Mechanobiol.* 2008;8(5):345–58.

[44] Rashid B, Destrade M, Gilchrist MD, Inhomogeneous deformation of brain tissue during tension tests. *Comput Mater Sci* (in press). 2012: DOI:10.1016/j.commatsci.2012.05.030.

[45] Pervin F, Chen WW. Effect of inter-species, gender, and breeding on the mechanical behavior of brain tissue. *NeuroImage.* 2011;54(1):S98–S102.

[46] Prange MT, Meaney DF, Margulies SS. Defining brain mechanical properties: effects of region, direction and species. in: *Proc 44th Stapp Car Crash Conference.* 2000:205–13.